Laser-Induced Slippery Liquid-Infused Surfaces with Anticorrosion and Wear Resistance Properties on Aluminum Alloy Substrates

Qianqian Cai, Jinkai Xu,* Zhongxu Lian,* Zhanjiang Yu, Huadong Yu, Shen Yang, and Jian Li

ACCESS | Metrics & More | Article Recommendations

ABSTRACT: Slippery liquid-infused surfaces (SLISs) are developed as a potential alternative to superhydrophobic surfaces (SHSs) to resolve the issues of poor durability in corrosion protection and wear resistance. In this work, we used a simple laser processing technology to prepare a SLIS on the aluminum alloy (7075) surface. The superhydrophobicities of the modified surface and the oil film formed by liquid injection make the corrosive medium difficult to directly contact the surface and thus have a significant effect on corrosion resistance. The water and oil repellent SLIS exhibits durable corrosion resistance and excellent tribological properties compared with the SHS. The anticorrosion and wear resistance performances provided by the composite film have been assessed by multiple methods including the electrochemical test, immersion test, and friction wear test. The results indicate that compared to the bare surface, laser-ablated surface (LAS), and fluoroalkyl silane-modified SHS, the SLIS composite coating has better corrosion resistance and wear resistance, which is of great significance to expand the potential applications of 7075 aluminum alloys. The work provides a research basis for expanding the practical application of SLISs in complex environments.
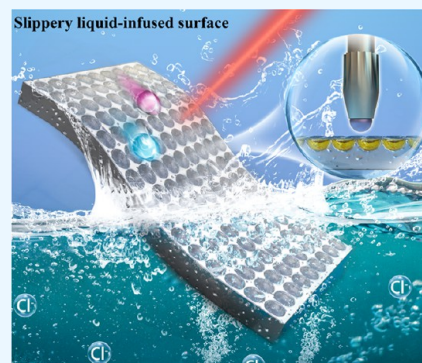
1. INTRODUCTION

Aluminum (Al) alloy materials are indispensable in the industrial field due to their high strength, low density, and good processing performance, which are widely used in various fields such as electronic engineering, petrochemical engineering, and aerospace.[1−4] However, corrosion occurs when all alloy materials are exposed to the atmosphere, seawater, soil, and other media, resulting in equipment damage and huge economic losses.[5−9] Al has high electrochemical activity, and Al alloys are easy to be corroded in many application environments, especially in chloride solutions, which seriously restricts their promotion and applications in various fields.[10,11] Therefore, how to effectively reduce the surface corrosion of materials has become an important issue in the surface treatment of Al alloy materials.[12−14]

In recent years, with the in-depth study of superhydrophobic surfaces (SHSs), scholars have found that metal materials with special wettability are of great significance in the field of corrosion protection.[15−17] The SHS prevents the corrosive liquid from coming into contact with the material surface due to its special liquid repellent property, which is a method for effectively protecting the Al alloy substrate from corrosion.[18−20] In practical applications, it is found that the superhydrophobic property of coatings is not stable, which will lead to the failure of superhydrophobic coatings under high temperature, high pressure, or surface damage.[21] Compared with the SHS, the air layer in the micro/ nanostructures is replaced by the lubricating liquid, forming

a more stable solid−liquid composite layer. The slippery liquid-infused surface (SLIS) is super slippery, liquid repellent, and stable even under high-temperature and high-pressure conditions, and the surface has self-healing and repairability after physical damage.[22−25] On this basis, the researchers have found that the SLIS is more conducive for improving the surface corrosion performance due to its superior liquid repellent properties.[26−28] In addition, the lubricant on the SLIS can form a lubricating film and reduce the friction and extrusion damage on the material surface during use.[29] Therefore, constructing a SLIS is an important method to further solve the problems of corrosion and wear of Al alloy materials.[30,31]

To date, researchers have proposed many methods for preparing SLISs, such as electrochemical etching/anodizing and chemical etching methods, sol−gel method, spraying method, and layer-by-layer self-assembly method.[32−35] However, most of the methods have various disadvantages such as the lack of safety, environmental pollution, and wear of coatings. Specifically, electrochemical etching/anodizing and
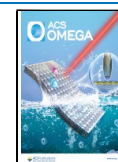
chemical etching methods involve a large amount of strong acid and alkali, and an easy-to-scatter organic solvent needs to be used when applying the spraying method.[36−38] In this case, the safety of operators and the pollution of the environment cannot be ignored. For the sol−gel method, spraying method, and layer-by-layer self-assembly method, the obtained coating and material substrate are mainly mechanically bonded, so the bonding strength to the surface is low, which limits the actual use of SLISs.[39,40]

Recently, lasers have proven to be one of the most powerful tools in the field of advanced micro/nanomanufacturing, which has been successfully applied in the field of surface science to regulate the wettability of material surfaces.[41−43] To date, the femtosecond laser processing technology has been used as one of the main preparation methods of SLISs. Compared with femtosecond laser technology, nanosecond laser technology has the advantages of low cost, high efficiency, and few requirements for environmental conditions, which is more suitable for the industrial production of SLISs.[44−46] In this work, a simple method has been used to produce a corrosion resistance SLIS on the Al alloy substrate. Besides, the array pit structures have also been constructed by nanosecond laser technology. The obtained microstructures can be modified by low-surface-energy materials to fabricate an SHS, and the SLIS can be obtained by infusing lubricant into the SHS. The corrosion resistance and wear resistance of the SHS and SLIS were compared and evaluated.

2. EXPERIMENTAL SECTION

2.1. Materials. Al alloy (7075) samples were purchased from Northwest Institute of Nonferrous Metal Company, and the composition is shown in Table 1. *n*-Dodecane and

Table 1. Elements Composition of 7075 Al Alloy, wt %

| Si	Cu	Mg	Zn	Mn	Ti	Cr	Fe	Al
0.40	0.10	4.0	0.25	1.0	0.15	0.05	0.40	balance

hexadecane were purchased from Sigma-Aldrich. Absolute ethanol, acetone glycerol, ethylene glycol, olive oil, dichloroethane, and chloroform were from Jilin Hao Di Chemical Reagent Ltd. Fluoroalkyl silane (1*H*,1*H*,2*H*,2*H*-perfluorooctyltriethoxysilane) was purchased from Aladdin.

2.2. Fabrication. An Al alloy sheet was cut into 14 mm × 14 mm × 2.5 mm samples using a wire-cutting machine

(HA400U) in a numerical control servo system. They were mechanically polished using an abrasive paper (400, 800, 1500 grit) and then ultrasonically cleaned in acetone (99%), absolute ethanol (99%), and deionized water for 10 min. The Al alloy surface roughness was 75 ± 5 nm measured by an atomic force microscope (AFM, Anton Paar Tosca 200, Austria). The morphology of the Al alloy surface was formed using a Q-switched nanosecond laser marking system with a wavelength of 1064 nm and a pulse width of 100 ns using the array point scanning process. The parameters of Q frequency, laser fluence, and scanning speed were 20 kHz, 22.95 J·cm^{-2}, and 500 mm·s^{-1}, respectively. After the laser ablation, the laser-ablated surfaces (LASs) were immersed into a fluoroalkyl silane/ethanol solution with a mass fraction of 1 wt % to obtain superhydrophobicity. Finally, the as-prepared samples were immersed into the perfluorinated lubricant (Dupon Krytox GPL103) for 1 h to obtain the SLISs, and the sample was then tilted at an angle of ~60° for 4 h to get rid of the excess perfluorinated lubricant. The whole preparation process for the SLIS is depicted in Scheme 1.

2.3. Characterization. A scanning electron microscope (SEM, FEI Quanta 250) was used to observe the surface morphology of the sample. The optical images of the samples were obtained using a digital camera (EOS M3). The chemical composition of the samples was characterized by energy-dispersive X-ray spectroscopy (EDS, X-Max). The chemical composition of the sample surface was analyzed by the plane scanning mode, the scanning area was 110 μm × 80 μm, and the quantification method of EDS was mass percentage. X-ray photoelectron spectroscopy (XPS, Thermo Escalab 250) was conducted to examine the chemical states of the surface. The sample was placed in an ultrahigh vacuum chamber of the XPS instrument to perform the measurement. The binding energy was calibrated by setting the C 1s line at 284.6 eV. The XPS data were analyzed by Avantage software. A contact angle measuring instrument (OCA20, Germany) was used to measure the surface wettability of water and oil droplets; 5 μL water and oil droplets were used separately to measure the contact angle (CA), sliding angle (SA), and sliding state of the droplets on different sample surfaces and three values were obtained on each sample. When measuring the SA, the droplet was kept still on the sample surface, and the worktable was rotated at a speed of 1.0° per second until the droplet rolled. The rotation angle of the worktable was the SA of the droplet.

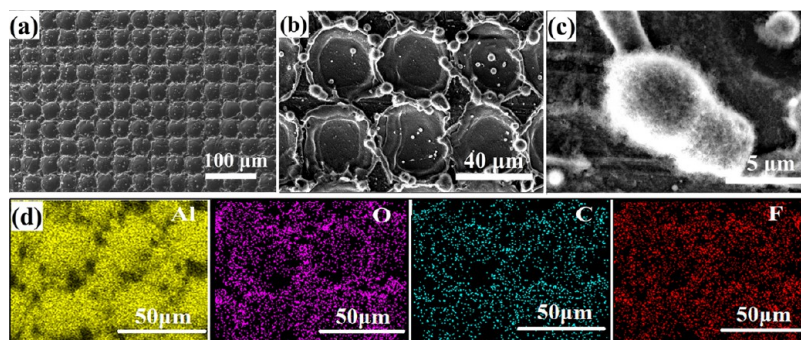**Scheme 1. Preparation Process of the SLIS**
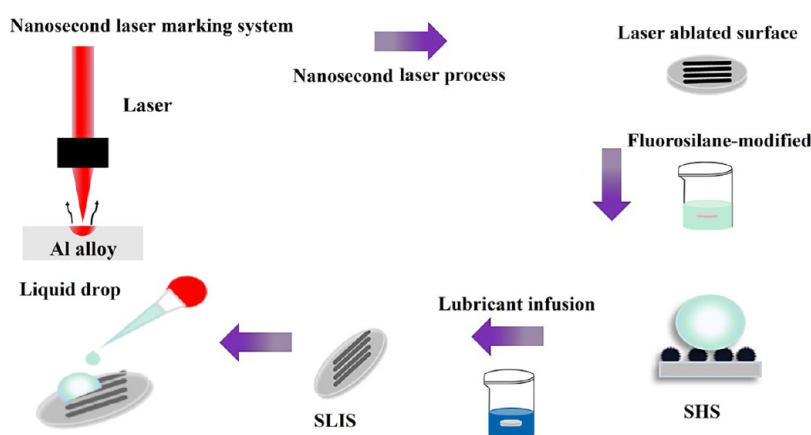
Figure 1. SEM images of the Al alloy surface after laser processing: (a−c) SEM images of the laser-ablated Al alloy surface and (d) element distribution maps of the fluoroalkyl silane-modified SHS.
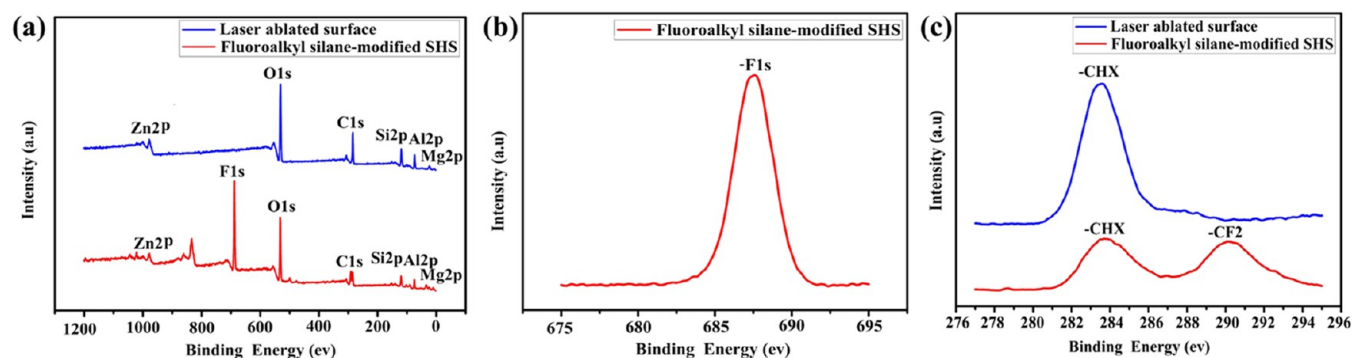

Figure 2. High-resolution XPS spectra of the LAS and fluoroalkyl silane-modified SHS.
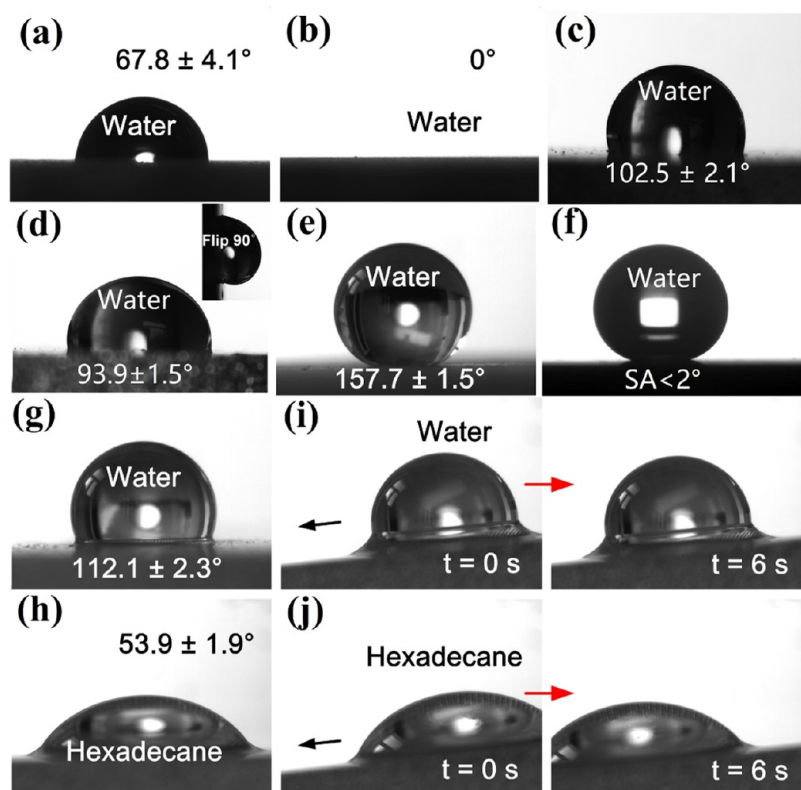

Figure 3. Wetting states of water and hexadecane droplets to different Al alloy surfaces: (a−f) water droplets on the bare surface, LAS, hydrophobic surface, bare Al alloy surface injected with the perfluorinated lubricant, and fluoroalkyl silane-modified SHS. (g, h) CAs and (i, j) sliding states of (g, i) water and (h, j) hexadecane droplets to the SLIS.
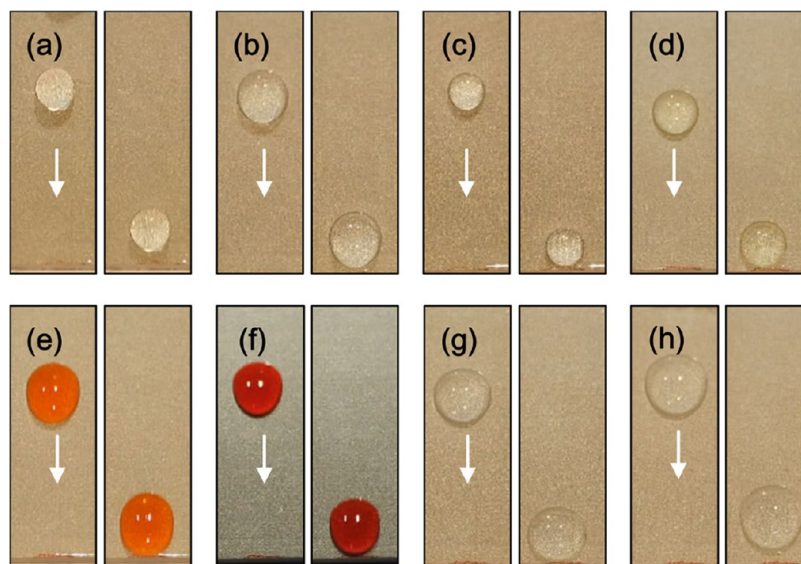
Figure 4. Sliding states of different types of droplets on SLIS (inclination angle of 10°): (a) water, (b) glycerol, (c) ethylene glycol, (d) olive oil, (e) dichloroethane, (f) chloroform, (g) *n*-dodecane, and (h) hexadecane.

A digital camera (EOS M3) was used to characterize the sliding state of the water and oil droplets.

2.4. Corrosion Test. The corrosion resistance of the surface was evaluated by a potentiodynamic polarization (PP) curve test, an electrochemical impedance spectroscopy (EIS) test, and salt water immersion at room temperature using a 3.5 wt % NaCl solution. An electrochemical workstation (Zahner Zennium, Germany) was used to test the electrochemical corrosion behavior of the sample in the 3.5 wt % NaCl solution. The test was carried out under a standard three-electrode system, the sample was used as a working electrode, and its exposed surface area was 1 cm². Before the electrochemical test, the test solution was degassed by bubbling pure argon to eliminate the influence of dissolved oxygen in the 3.5 wt % NaCl solution on the test.

During the entire test, the solution temperature was maintained at 25 ± 1 °C. For the PP curve test, the scanning rate was 1 mV·s⁻¹. The corrosion potential (E_{corr}), corrosion current density (I_{corr}), and anodic/cathodic Tafel polarization slopes β_a/β_c on the surface were obtained by the Tafel extrapolation method. For the EIS test, the whole process was carried out under the open circuit voltage, the frequency was from 100 kHz to 10 mHz, and the sinusoidal signal was disturbed to 10 mV. In the salt water immersion experiment, the surface was immersed into the 3.5 wt % NaCl solution, and the morphology and chemical composition before and after immersion were analyzed.
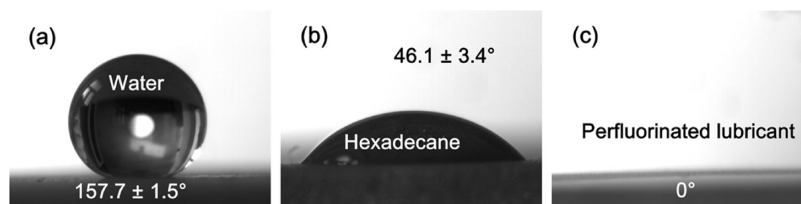
2.5. Friction and Wear Tests. Tribology testing was conducted using a multifunctional friction and wear testing machine (Rtec MFT-3000) to investigate the tribological performance of the sample surface. The experimental parameters were a temperature range of 18−20 °C, an ambient relative humidity range of 45−50%, a load of 0.5 N, and a sliding speed of 0.3 mm·s⁻¹. During the experiment, a 4.0 mm diameter SUS440C stainless steel ball was used as a mating part with a reciprocating travel of 3 mm, and the test time was 1800 s. The sample was fixed on the worktable, three different positions on the surface of the sample were taken, and the friction and wear tests were performed on the sample. The SUS440C stainless steel ball needs to be replaced for each test.

3. RESULTS AND DISCUSSION

3.1. Surface Morphology, Chemical State, and Wetting Behavior. Figure 1 shows the SEM images of the Al alloy surface after laser processing. After laser processing, it can be seen that there is an array pit structure on the surface, and a convex structure is formed around the pit due to the accumulation of molten deposits on each other (Figure 1a). By further magnifying the SEM images (Figure 1b,c), it is observed that there are nanoscales on the surface of the microscale pits and convex structures, which constitute micro/nanoscale composite structures of the laser-machined Al alloy surface. The F element was observed on the fluoroalkyl silane-modified SHS based on the EDS results and distributed evenly on the entire coating, as shown in Figure 1d.

XPS was used to further analyze the chemical states of the surface elements of the samples before and after fluoroalkyl silane modifications. Figure 2a shows the high-resolution XPS spectra of the LAS and the fluoroalkyl silane-modified SHS. Compared with the LAS, the fluoroalkyl silane-modified SHS presents a strong peak of F 1s at 688.4 eV (Figure 2b), and the peak corresponding to −CF2 is observed in Figure 2c. The results indicated that the fluoroalkyl silane-modified SHS was coated with fluoroalkyl silane.[47,48]

Figure 3 shows the wetting states of water and hexadecane droplets to different Al alloy surfaces. From the images (Figure 3a,b), the bare Al alloy surface is hydrophilic (67.8 ± 4.1°), while the laser-ablated Al alloy surface is superhydrophilic (0°). The Wenzel model can explain the change in wettability.[49] The actual solid−liquid contact area is larger than the apparent contact area, so the CA becomes smaller as the surface roughness increases.[50] After modification with fluoroalkyl silane, a water droplet on the base Al alloy surface exhibits hydrophobicity with a CA of 102.5 ± 2.1° (Figure 3c). Fluorination treatment can reduce the surface free energy and increase the hydrophobicity of the surface, but the CA of the water droplet is not greater than 120°.[51,52] The perfluorinated lubricant is injected into the hydrophobic surface and the CA is 93.9 ± 1.5°. When the surface is turned 90°, the water droplets still adhere to the surface (Figure 3d). A water droplet on the fluoroalkyl silane-modified LAS exhibits superhydro-

Scheme 2. CAs of Droplets on a Fluoroalkyl Silane-Modified Laser-Machined Surface[a]

[a](a) Water, (b) hexadecane, and (c) perfluorinated lubricant.

phobicity, with a CA of 157.7 ± 1.5° and an SA of less than 2° (Figure 3e,f). The superhydrophobic properties of the surface are the result of the interaction between the micro/nanostructure and the chemical composition.[53,54] Figure 3g–j shows the CAs and sliding states of the droplets to the SLIS. The CAs of the water and hexadecane droplets are 112.1 ± 2.3 and 53.9 ± 1.9°, respectively, and the sliding speeds of the two droplets to the surface with an inclination angle of 5° are 0.14 ± 0.01 and 0.31 ± 0.02 mm·s^{-1}, respectively. In addition, the results of different types of oil droplets (glycerin, ethylene glycol, olive oil, dichloroethane, chloroform, n-dodecane, and hexadecane) moving on the SLIS are shown in Figure 4, and it can be seen that various droplets easily slid over the surface with an inclination angle of 10°. According to the relevant criteria of SLIS, the substrate of micro/nanostructure is conducive to the complete wetting and adhesion of the lubricating liquid.[55,56] After the perfluorinated lubricant penetrates and wets the micro/nanostructure, the formed lubricating film prevents the droplets from directly contacting the surface of the substrate, resulting in super slippery properties. Therefore, when the surface is tilted at a certain angle, the droplets that land on the SLIS can easily slide off.

The shape of the water droplet on the fluoroalkyl silane-modified LAS was close to a circular shape (157.7 ± 1.5°), and the CA of the hexadecane droplet to the surface was 46.1 ± 3.4° (Scheme 2a,b). The perfluorinated lubricant droplet diffused rapidly on the surface, and the CA was 0°, which was manifested as superoleophilicity for the perfluorinated lubricant (Scheme 2c). The results show that the chemical affinities of the perfluorinated lubricant and the surface are higher than those of water or other oil droplets (glycerol, ethylene glycol, olive oil, dichloroethane, chloroform, n-dodecane, and hexadecane) and the surface. According to the theory of SLIS, when water or other oil droplets fall onto the SLIS injected by the perfluorinated lubricant, the formed perfluoro-oil film prevents the droplets from passing through, avoiding direct contact with the surface and forming a stable oil−liquid−solid−gas contact zone.

To evaluate the air stability of the SLIS and verify whether the surface lubricant evaporates over time and the performance of SLIS is invalid, the air stability of the SLIS is tested. The sample is placed in the air for 21 days, and the CAs and SAs are measured every 3 days (Figure 5). The CAs are maintained at 112 ± 3.5°, and the SAs are less than 5°, indicating that the prepared SLIS has excellent air stability.

3.2. Corrosion Resistance. Figure 6 shows the open circuit potential (OCP) curves of the bare surface, LAS, fluoroalkyl silane-modified SHS, and SLIS in a 3.5 wt % NaCl solution. It can be seen that after 1800 s, the OCP values of different sample surfaces have reached a relatively stable state, and the OCP values are in the following order: bare surface > fluoroalkyl silane-modified SHS > SLIS > LAS. The electro-
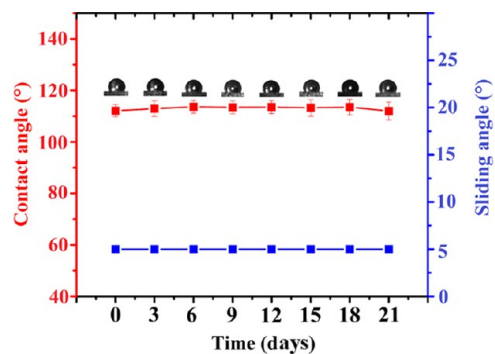

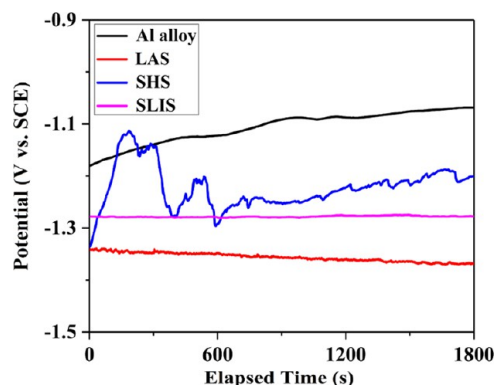**Figure 5.** Wettability of the SLIS placed in the air for different days.

Figure 6. OCP curves of Al alloy surfaces treated under different processing conditions.

chemical potential of the bare surface is the highest, and the LAS is the lowest. In addition, the OCP curve of the fluoroalkyl silane-modified SHS fluctuates greatly in the early stage, which may be caused by the superhydrophobicity of the surface.

Figure 7 shows the PP curves of the bare surface, LAS, fluoroalkyl silane-modified SHS, and SLIS. Table 2 shows the E_{corr} and I_{corr}, and the anodic/cathodic Tafel polarization slopes β_a/β_c of the different surfaces. The Stern−Geary equation is used to calculate the polarization resistance R_p of different sample surfaces[57]

$$R_p = \frac{\beta_a \times \beta_c}{2.303 \times I_{corr} \times (\beta_a + \beta_c)} \frac{1}{A} \quad (1)$$

where A is the exposed area of different samples, $A = 1$ cm^2.

Table 2 shows the polarization resistance R_p values of different sample surfaces in the following order: $R_{p\text{-SLIS}}$ (1.16 × 10^5 Ω) > $R_{p\text{-SHS}}$ (3.15 × 10^3 Ω) > $R_{p\text{-Al}}$ (2.92 × 10^2 Ω) > $R_{p\text{-LAS}}$ (1.60 × 10^2 Ω). The corrosion current densities of LAS (2.62 × 10^{-4} A·cm^{-2}) were higher than that of the bare surface (1.01

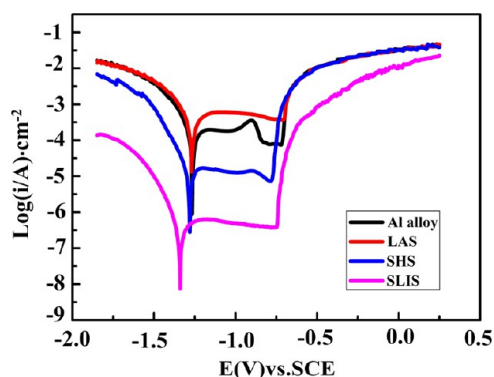**Figure 7.** Polarization curves of Al alloy surfaces treated under different processing conditions.

Figure 8. Nyquist plots of Al alloy surfaces treated with different conditions.

$\times$ 10^{-4} A·cm^{-2}), indicating that the laser processing reduced the corrosion resistance of the Al alloy surface. According to the analysis, the LAS was superhydrophilic, which caused the chloride ion in the corrosion solution to directly contact the surface and promoted the occurrence of the corrosion reaction, leading to a decrease in surface corrosion resistance. After modification with fluoroalkyl silane, the I_{corr} of the LAS was significantly reduced to 7.55 × 10^{-6} A·cm^{-2}, suggesting that the fluoroalkyl silane modification increased the corrosion resistance of the surface in addition to improving the hydrophobicity. For the SLIS, I_{corr} was 1.88 × 10^{-7} A·cm^{-2}, and it was reduced by 3 orders of magnitude compared with that of the bare surface. This excellent corrosion resistance property is due to the fact that the liquid lubricant completely covered the fluoroalkyl silane-modified SHS, inhibiting electron transfer between the substrate and the etching solution. The corresponding corrosion protection efficiency (P_{EF}) is calculated as follows[58]

$$P_{EF} = \frac{R_{cp} - R_{pp}}{R_{cp}} \times 100\%$$

(2)

where R_{pp} refers to the polarization resistance of the Al alloy substrate, and R_{cp} is the polarization resistance of the Al alloy surfaces treated with different conditions. According to eq 2, the corrosion protection efficiencies of the fluoroalkyl silane-modified SHS and the SLIS are 90.73 and 99.75%, respectively.

Figure 8 shows the Nyquist plots of the bare surface, LAS, fluoroalkyl silane-modified SHS, and SLIS. It is found that the SLIS has the largest diameter in the capacitive impedance arc, followed by SHS and Al alloy substrate and LAS in the NaCl solution. As a matter of fact, the diameter of the capacitive impedance arc is proportional to the corrosion resistance of the sample. In a specific way, an increasing diameter of the capacitive impedance arc means an increase in the resistance of the electrochemical reaction. The Al alloy substrate's Nyquist plot is composed of dual capacitive impedance arcs in the high- and low-frequency regions. The Nyquist plot of LAS shows a
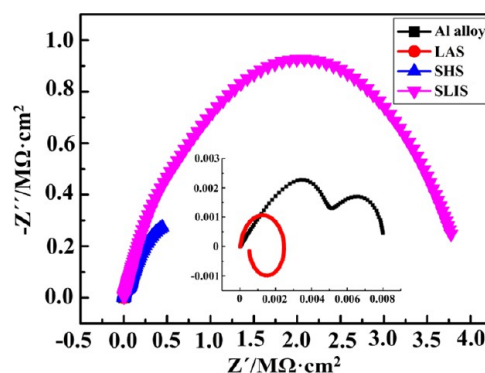
capacitive impedance arc in the high-frequency region and an inductive impedance arc in the low-frequency region. In the pitting corrosion model of Al alloy, inductive impedance means the occurrence of the pitting corrosion, and therefore, the low-frequency inductive impedance arc represents that the pitting corrosion occurs on the LAS. It is concluded that both SLIS and SHS are capable of improving the corrosion resistance of the Al alloy substrate. For the SLIS surface, it can be explained that the lubricant present on the SLIS surface is helpful to isolate the corrosion media from the Al alloy substrate, especially in water because the lubricant is incompatible with water and can be caught for a long period of time, slowing down the process of corrosion. The sample with SHS coating is immersed in the NaCl solution, and hence, a large amount of air is trapped in the micro/nanostructures of the coating. The air layer makes it possible to reduce the contact area between the NaCl solution and the coating, delaying the occurrence of corrosion.

As shown in Figure 9a, the low-frequency impedance modulus (|Z|) value is 10$^{6.5}$ Ω·cm^2 and is significantly higher than 10$^{3.9}$ Ω·cm^2 of the bare surface, which is an increase of about 3 orders of magnitude. It is well known that the increased |Z| value means an increase in corrosion resistance. The |Z| value of the LAS is the smallest (10$^{2.7}$ Ω·cm^2), indicating that the LAS is unacceptable in corrosion resistance. According to the analysis, the LAS is superhydrophilic, which causes the chloride ions in the corrosion solution to directly contact the surface and promotes the occurrence of the corrosion reaction. For the fluoroalkyl silane-modified SHS, the |Z| is significantly increased, and the |Z| value is 10$^{5.7}$ Ω·cm^2.

As shown in Figure 9b, all samples have two time constants. The time constant in the low-frequency region represents local corrosion that occurred on the surface, and the time constant in the medium-frequency region means the charge transfer resistance (R_{ct}) and double electric layer capacitance (CPE$_{dl}$) during the process of corrosion. The inhibiting effect generated by the uniform and dense coating results in the appearance of a

Table 2. E_{corr} and I_{corr} of Al Alloy Surfaces Treated under Different Processing Conditions in the NaCl Solution

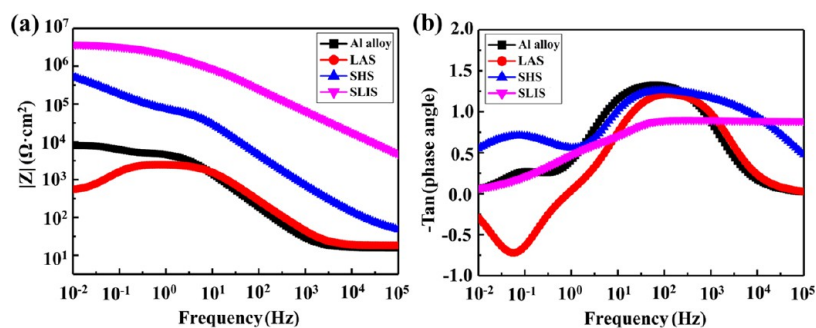| sample	E_{corr} (V)	I_{corr} (A·cm^{-2})	P_{EF} (%)	β_a (mV·dec^{-1})	β_c (mV·dec^{-1})	R_p (Ω)
bare Al alloys	−1.27	1.01 × 10^{-4}		314	86.8	2.92 × 10^2
LAS	−1.27	2.62 × 10^{-4}		326	137	1.60 × 10^2
fluoroalkyl silane-modified SHS	−1.28	7.55 × 10^{-6}	90.73	159	83.7	3.15 × 10^3
SLIS (40 μm)	−1.34	1.88 × 10^{-7}	99.75	144	77.4	1.16 × 10^5

Figure 9. Bode plots of Al alloy surfaces treated with different conditions.

high-frequency capacitance loop.[59] On the other hand, two time constants are available to the Al alloy substrate, LAS, and fluoroalkyl silane-modified SHS. One is in the low-frequency region and the other is in the medium-frequency region. The two time constants of SLIS are in the medium- and high-frequency regions.

Zahner analysis software is used to fit the electrochemical data so as to explore the process of coating corrosion. The equivalent circuit is obtained, as shown in Figure 10, where R_s
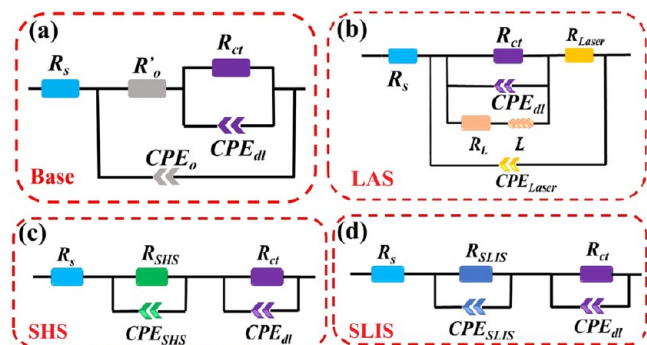

Figure 10. Equivalent circuit models for the EIS fitting of different samples: (a) bare surface, (b) LAS, (c) fluoroalkyl silane-modified SHS, and (d) SLIS.

means the solution resistance between the sample and the reference electrode. R_{ct} and CEP_{dl} represent the charge transfer resistance and double electric layer capacitance between the coating and the substrate, respectively. R'_o is the additional resistance of the solution within the pit.[60] CEP_o is the double electric layer capacitance of the oxide layer. R_{SLIS} and CEP_{SLIS} are the resistance and capacitance of the oil film. R_{SHS} and CEP_{SHS} refer to the resistance and capacitance of the SHS. R_{Laser} and CEP_{Laser} are the resistance and capacitance of the LAS, and the inductance element L is connected in series in the R_L circuit, which represents the inductance behavior due to the pitting corrosion. CPE_{dl} is represented by the constant phase element (CPE) Q. The value of CPE_{dl} can be calculated by Brug's formula[61,62]

$$C_{dl} = Q_{dl}^{1/n}\left(\frac{1}{R_s} + \frac{1}{R_{ct}}\right)^{n-1/n}$$

(3)

where Q is the value of CPE and n is the CPE's dimensionless exponent.[63] When $n = 1$, Q is equivalent to an ideal capacitor. It is observed from the fitting results listed in Table 3 that R_{ct} is increased from 2.85 kΩ·cm^2 of the Al alloy substrate to 122 kΩ·cm^2 of the SLIS, and the CPE_{dl} value is decreased 4 orders of magnitude accordingly. Generally, the charge transfer resistance is associated with corrosion. The higher the charge transfer resistance, the lower the corrosion rate. A change in the CPE_{dl} value illustrates the permeation behavior of the electrolyte on the coating, and the increased corrosion solution permeated into the coating causes an increase in the CPE_{dl} value.[63] It can be concluded that the SLIS plays a significant role in protecting the Al alloy substrate from the corrosion of chloride ions.

The corrosion resistance of the surface was further investigated by immersing the sample in the 3.5 wt % NaCl solution. Figure 11 shows the optical photographs of the bare
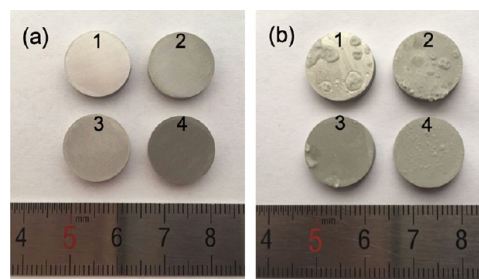

Figure 11. Optical photographs of Al alloy surfaces treated with different conditions before (a) and after (b) immersing in the 3.5 wt % NaCl solution for 21 days. Among them, sample 1 is the bare surface, sample 2 is the LAS, sample 3 is the fluoroalkyl silane-modified SHS, and sample 4 is the SLIS.

surface, LAS, fluoroalkyl silane-modified SHS, and SLIS before and after immersion. Figure 11a shows that the surfaces of the four samples that are not immersed are smooth and clean. As shown in Figure 11b, after immersion for 21 days, it can be

Table 3. Fitting Results of the EIS Data of Different Samples in the 3.5 wt % NaCl Solution

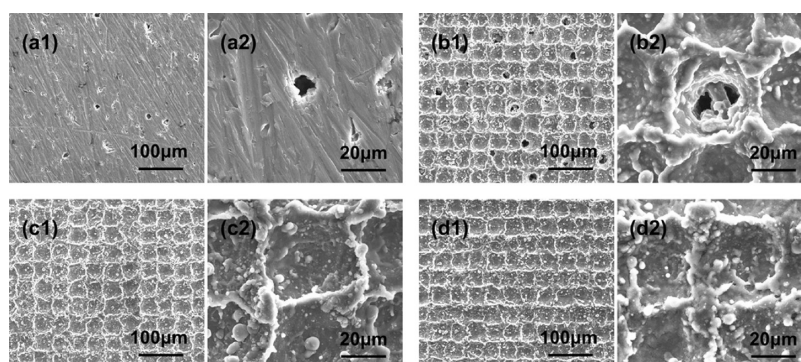| sample	R_{ct} (kΩ·cm^2)	Q_{dl} (Ω^{-1}·s^{-n}·cm^{-2})	n_{dl}	CEP_{dl} (μF·cm^{-2})	R_{coat} (kΩ·cm^2)	Q_{coat} (Ω^{-1}·s^{-n}·cm^{-2})
bare Al alloys	2.85	7.64×10^{-4}	1	7.64×10^{-4}	5.20	1.50×10^{-5}
LAS	2.09	5.68×10^{-6}	0.815	7.07×10^{-7}	0.41	7.10×10^{-6}
fluoroalkyl silane-modified SHS	44.6	7.82×10^{-7}	0.958	4.91×10^{-7}	1.02×10^3	8.16×10^{-6}
SLIS (40 μm)	122	6.17×10^{-8}	1	6.17×10^{-8}	3.88×10^3	1.14×10^{-7}

Figure 12. SEM images of Al alloy surfaces treated with different conditions after immersing in the 3.5 wt % NaCl solution for 21 days: (a) bare surface, (b) LAS, (c) fluoroalkyl silane-modified SHS, and (d) SLIS.

seen that there are many salt deposits on the bare and LASs. In contrast, the contaminants on the fluoroalkyl silane-modified SHS and the SLIS are reduced, and no significant signs of corrosion are observed. Also, the presence of an oil film is observed on the SLIS, demonstrating superior corrosion resistance.

Figure 12 shows the SEM images of the bare surface, LAS, fluoroalkyl silane-modified SHS, and SLIS after being immersed in the 3.5 wt % NaCl solution. As shown in Figure 12a, corrosion holes with a diameter of about 10 μm appeared on the bare Al alloy surface. For the LAS, after being immersed for 21 days into the corrosive solution, it is found that the number of corrosion holes increased, and the diameter increased to about 20 μm (Figure 12b), indicating that the corrosion of LAS is significant. For the fluoroalkyl silane-modified SHS and the SLIS, the morphology did not change (Figure 12c,d), indicating that the two surfaces have good stability in the 3.5 wt % NaCl solution. According to the analysis, the superhydrophobicity of the modified surface and the oil film formed by liquid injection make the corrosive medium difficult to directly contact the surface and thus produce a significant anticorrosion effect.

Table 4 shows the changes of the elements Al, O, F, Na, and Cl on the bare surface, LAS, fluoroalkyl silane-modified SHS,

Table 4. Changes of Elements Al, O, F, Na, and Cl Before and After Corrosion of Al Alloy Surfaces

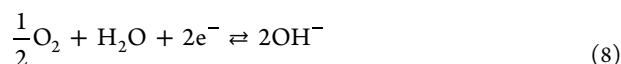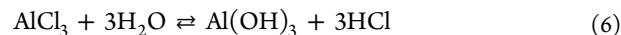| sample	time (days)	element composition and content (wt %)				
		Al	O	F	Na	Cl
bare Al alloys	0	98.3	1.7			
bare Al alloys	21	92.1	5.2		0.9	1.8
LAS	0	93.4	6.6			
LAS	21	76.1	19.4		1.7	3.2
fluoroalkyl silane-modified SHS	0	90.2	6.9	3.0		
fluoroalkyl silane-modified SHS	21	89.0	7.1	2.9	0.2	0.8
SLIS (40 μm)	21	89.8	6.9	3.0	0.1	0.2

and SLIS before and after the samples were immersed in the 3.5 wt % NaCl solution for 21 days. For the bare Al alloy surface, the weight percentage of element Al decreased from 98.3 to 92.1%, while the increase of element O (from 1.7 to 5.2%) and new elements Na and Cl (weight percentages of 0.9 and 1.8%, respectively) is observed on the surface, indicating

that the bare surface is corroded by the NaCl solution. For the LAS, fluoroalkyl silane-modified SHS, and SLIS, the elements Na and Cl are found on all three surfaces, and the weight percentage of element O shows an increase after 21 days. The difference is that the weight percentages of elements O, Cl, and Na on the LAS are 19.4, 1.7, and 3.2%, respectively, which are more than those of the bare surface after being immersed in the NaCl solution, indicating that the LAS has more serious corrosion. However, the fluoroalkyl silane-modified SHS and the SLIS have little change in element O, and elements Cl and Na are also less, caused by residual chloride on the surface after immersion in the NaCl solution for a long period of time. Simultaneously, element F is also detected on the fluoroalkyl silane-modified SHS and SLIS, and their contents are 2.9 and 3.0%, respectively, which are unchanged compared to the unsoaked fluoroalkyl silane-modified SHS (3.0%). The results show that the low-surface-energy materials are not damaged, indicating that the fluoroalkyl silane-modified SHS and SLIS are substantially not corroded after being immersed in the 3.5 wt % NaCl solution for 21 days.

3.3. Corrosion Mechanism. It can be seen from the above corrosion test that in the NaCl solution, the chloride ion erodes the oxide film on the surface of the Al alloy substrate, irregular pits appear on the surface of the Al alloy, and pitting corrosion occurs (Figure 12).[60] The anodic reaction is mainly as follows[64]

$$Al \rightleftarrows Al^{3+} + 3e^- \tag{4}$$

$$Al^{3+} + 3H_2O \rightleftarrows Al(OH)_3 + 3H^+ \tag{5}$$
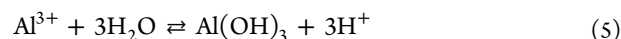
According to eq 5, the acidity of the anode position is enhanced, and the chloride ion promotes the anodic dissolution of Al to form aluminum chloride. The following reactions may occur at the cathode

$$AlCl_3 + 3H_2O \rightleftarrows Al(OH)_3 + 3HCl \tag{6}$$

$$3H^+ + 3e^- \rightleftarrows \frac{3}{2}H_2 \tag{7}$$

$$\frac{1}{2}O_2 + H_2O + 2e^- \rightleftarrows 2OH^- \tag{8}$$

In the corrosion solution, the bare surface and the LAS are hydrophilic, and the corrosive solution is in direct contact with the surface of the sample, resulting in serious corrosion behavior. In addition, the micro/nanoscale composite structures of the LAS increase the real contact area between the corrosion solution and the surface of the sample, resulting
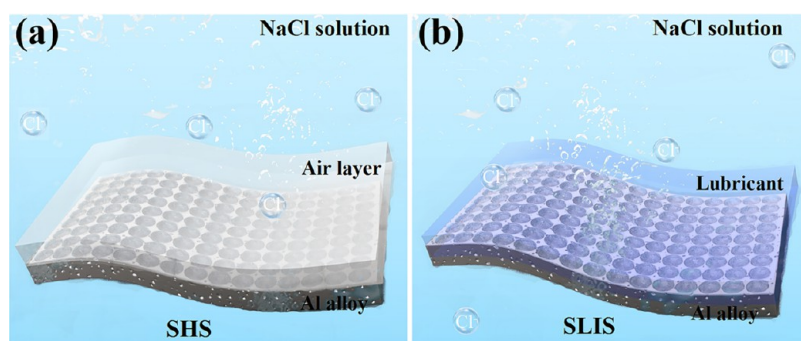
Figure 13. Schematic images of the corrosion-resistant mechanism model of the solid−liquid interface between the Al alloy surface and the 3.5 wt % NaCl solution under different treatment conditions: (a) fluoroalkyl silane-modified SHS and (b) SLIS.
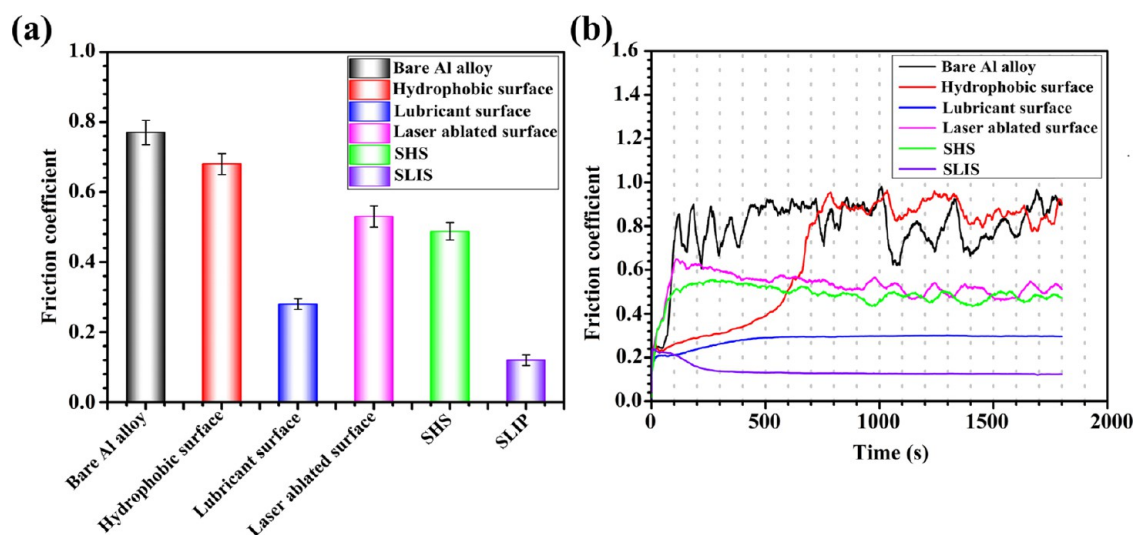

Figure 14. Average values of the friction coefficients of different sample surfaces.

in more serious surface corrosion. The fluoroalkyl silane-modified SHSs are superhydrophobic. When the fluoroalkyl silane-modified SHS is immersed in the corrosion solution, an air layer is formed on the surface, which can reduce the real contact area between the corrosion solution and the fluoroalkyl silane-modified SHS and effectively improve the corrosion resistance of the fluoroalkyl silane-modified SHS (Figure 13a).[65] However, in the corrosive solution, the super-hydrophobic property of SHS gradually disappeared under external pressure for a long time.[66] Compared with the fluoroalkyl silane-modified SHS, the air layer in the micro/ nanoscale composite structures is replaced by the lubricant to form a more stable solid−liquid composite layer. Especially in water, the lubricant stored in the micro/nanoscale composite structures is incompatible with water, effectively isolating the contact between the corrosion solution and the Al alloy substrate (Figure 13b). In addition, when the SLIS is damaged, the lubricant on the surface can quickly repair the damaged area under the surface energy-driven capillary action, providing more long-term and stable protection for the Al alloy substrate.[67]

3.4. Tribological Behaviors. Figure 14 shows the friction coefficient curves of different sample surfaces. It can be seen that the friction coefficient of the bare surface is the largest, reaching 0.77, and the friction coefficient of the SLIS is the smallest, about 0.12. The friction coefficient is reduced by 84.4% compared to the bare surface. At the beginning of the

friction test (0−700 s), the friction coefficient of the hydrophobic surface is relatively small. The fluoroalkyl silane modification reduces the free energy of the bare surface. Larger surface free energy corresponds to stronger adhesion, which leads to higher friction between the two surfaces.[68] But with the increase of the friction test time, the hydrophobic surface wears, and the friction coefficient gradually increases close to the friction coefficient of the bare surface. Compared with the bare surface and hydrophobic surface, the friction coefficient of the bare surface injected with the perfluorinated lubricant is smaller. This is because when the relative movement between the friction pairs occurs, the lubricant on the bare Al alloy surface adheres to the surface of the SUS440C stainless steel ball with a lubricating effect. Compared with the bare Al alloy surface, the friction coefficients of the LAS and fluoroalkyl silane-modified SHS are small, and the micropit structures on the LAS can store the wear debris generated during the friction process and reduce the contact between the wear debris and the substrate. However, the friction coefficient of the SHS is not significantly lower than that of the LAS. This is because the SHS wears and the superhydrophobic performance becomes invalid when the relative movement between the friction pairs occurs. Most surprisingly, the friction coefficient of the SLIS is significantly lower than that of the bare surface injected with the perfluorinated lubricant. When the friction pairs move relatively, the lubricant on the surface of the substrate spontaneously adheres to the surface of the stainless steel
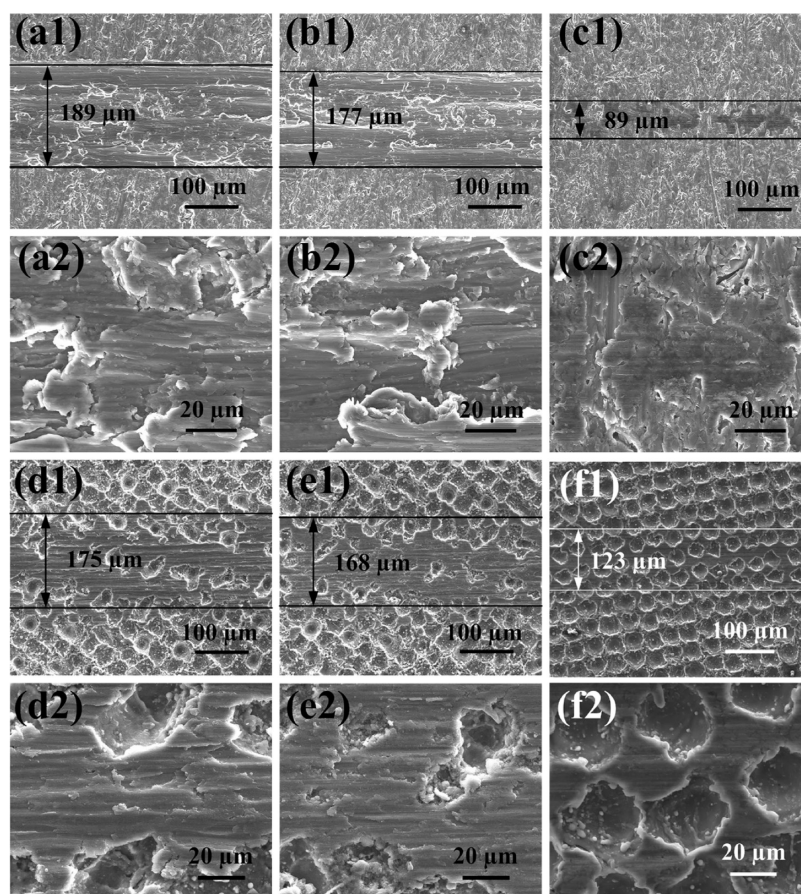
(a1) 189 μm 100 μm
(b1) 177 μm 100 μm
(c1) 89 μm 100 μm
(a2) 20 μm
(b2) 20 μm
(c2) 20 μm
(d1) 175 μm 100 μm
(e1) 168 μm 100 μm
(f1) 123 μm 100 μm
(d2) 20 μm
(e2) 20 μm
(f2) 20 μm

Figure 15. SEM images of the surfaces of different samples in the friction and wear tests: (a) bare surface, (b) hydrophobic surface, (c) bare Al alloy surface injected with the perfluorinated lubricant, (d) LAS, (e) fluoroalkyl silane-modified SHS, and (f) SLIS.

ball, providing a lubricating medium for the contact interface. However, with the continuous friction test, the substrate surface is not conducive to the storage of lubricant, and the lubricant on the surface is lost, which cannot continuously provide a lubricating medium for the contact interface, and the friction coefficient increases. In contrast, the micropit structures of the SLIS are more conducive to the storage of the lubricant, preventing the loss of the lubricant on the surface during frictional movement and providing continuous lubrication for the friction pair. The results show that the lubricating effect of the oil film and the storage function of the microstructures play an important role, and the phenomenon that the grinding debris adheres to the surface to increase the frictional force is avoided.

Figure 15 shows the SEM images of the surface wear of the bare surface, hydrophobic surface, bare Al alloy surface injected with the perfluorinated lubricant, LAS, fluoroalkyl silane-modified SHS, and SLIS. It can be seen in Figure 15a,b that the bare and hydrophobic surfaces have clear furrow structures in the sliding area along the sliding direction, and there is wear debris on the wear scar. The wear is mainly adhesive wear, with some abrasive wear. Moreover, there are cracks and depressions on the bare surface, which are consistent with the sliding direction (Figure 15a2).[69] The width of the wear scar to the bare surface is 189 μm, which has the largest value in the width of wear scars. The wear scar on the hydrophobic surface is relatively light, about 177 μm. The wear scar on the surface of the Al alloy substrate injected with the perfluorinated lubricant is 89 μm (Figure 15c), and there is

no obvious furrow structure on the surface, and the adhesion wear and the wear scar are significantly reduced. As shown in Figure 15d,e, the LAS and fluoroalkyl silane-modified SHS have larger values in the widths of wear scars, while the depths of wear scars to the two surfaces are significantly reduced relative to the bare surface described above, indicating that the microstructures of the laser processing improve the wear resistance of the surface to a certain extent.[70] The wear scar on the SLIS is 123 μm, indicating that the wear resistance of the Al alloy surface is significantly improved.

Based on the above results, the micropit structures constructed on the Al alloy surface by laser processing technology have proved to be capable of improving the tribological performance. The micropit structures on the LAS can store the wear debris, reducing the contact between the wear debris and the substrate during the friction process, thereby reducing the friction coefficient and the probability of the occurrence of abrasive wear. In addition, when the relative movement between the friction pairs occurs, the perfluorinated lubricant injected on the surface spontaneously adheres to the surface of the small ball and hence provides a lubricating medium for the contact surface. The combination of nanosecond laser processing and surface lubricant injection imparts excellent tribological properties to the Al alloy surface.

4. CONCLUSIONS

In this work, a SLIS with corrosion-resistant and wear-resistant properties has been obtained on the Al alloy surface by simple laser processing technology. The electrochemical test,

immersion test, and friction wear test were performed to investigate and evaluate the performance of the SLIS. The results showed that the SLIS exhibited excellent corrosion-resistant and tribological properties compared to the Al alloy substrate, LAS, and fluoroalkyl silane-modified SHS. Specifically, the results of the electrochemical experiment indicated that the I_{corr} of the SLIS was 1.88×10^{-7} A·cm^{-2}, decreased by 3 orders of magnitude compared to that of the Al alloy substrate. Besides, the |Z| value of the SLIS increased around 3 orders of magnitude, and its efficiency in corrosion resistance was significantly improved (P_{EF} = 99.75%). Even being immersed in the 3.5 wt % NaCl solution for 21 days, it still exhibited an excellent corrosion-resistant behavior. In the friction wear test, the friction coefficient of the SLIS surface was only 0.12, reduced by 84.4% compared to that of the Al alloy substrate, and the fewest scratches were found, having an excellent tribological property. The lubricant on the surface of the SLIS provided an opportunity to effectively prevent Cl$^-$ in the NaCl solution from corroding the Al alloy substrate, with a great potential for delaying the process of corrosion. Moreover, the array pit structures on the Al alloy surface were not only conducive to reducing the actual contact area between the SUS440C stainless steel ball and the surface but also capable of trapping wear debris and reducing the damage of the wear debris to the surface during scratching, leading to a reduced friction coefficient. During the relative movement, the lubricant on the surface adheres to the ball surface to provide lubrication. This research provides a novel and effective strategy for corrosion protection and wear resistance of Al alloy materials, and this method is simple in operation, low in cost, and easy to industrialize for high-volume manufacturing.

■ AUTHOR INFORMATION

Corresponding Authors

Jinkai Xu − *Ministry of Education Key Laboratory for Cross-Scale Micro and Nano Manufacturing, Changchun University of Science and Technology, Changchun 130022, China;* ⊙ orcid.org/0000-0002-5373-4564; Email: xujinkai2000@163.com

Zhongxu Lian − *Ministry of Education Key Laboratory for Cross-Scale Micro and Nano Manufacturing, Changchun University of Science and Technology, Changchun 130022, China;* Email: lianzhongxu@cust.edu.cn

Authors

Qianqian Cai − *Ministry of Education Key Laboratory for Cross-Scale Micro and Nano Manufacturing, Changchun University of Science and Technology, Changchun 130022, China*

Zhanjiang Yu − *Ministry of Education Key Laboratory for Cross-Scale Micro and Nano Manufacturing, Changchun University of Science and Technology, Changchun 130022, China*

Huadong Yu − *Ministry of Education Key Laboratory for Cross-Scale Micro and Nano Manufacturing, Changchun University of Science and Technology, Changchun 130022, China;* ⊙ orcid.org/0000-0003-0756-512X

Shen Yang − *Ministry of Education Key Laboratory for Cross-Scale Micro and Nano Manufacturing, Changchun University of Science and Technology, Changchun 130022, China*

Jian Li − *Ministry of Education Key Laboratory for Cross-Scale Micro and Nano Manufacturing, Changchun University of Science and Technology, Changchun 130022, China*

Complete contact information is available at:
https://pubs.acs.org/10.1021/acsomega.2c02360

Notes

The authors declare no competing financial interest.

■ REFERENCES

(1) Babaei, K.; Fattah-alhosseini, A.; Molaei, M. The effects of carbon-based additives on corrosion and wear properties of plasma electrolytic oxidation (PEO) coatings applied on aluminum and its alloys: A review. *Surf. Interfaces* **2020**, *21*, No. 100677.

(2) Esquivel, J.; Gupta, R. K. Review-corrosion-resistant metastable Al alloys: An overview of corrosion mechanisms. *J. Electrochem. Soc.* **2020**, *167*, No. 081504.

(3) Wang, R. T.; Xu, H.; Yao, Z. P.; Li, C. X.; Jiang, Z. H. Adhesion and corrosion resistance of micro-arc oxidation/polyurethane composite coating on aluminum alloy surface. *Appl. Sci.* **2020**, *10*, 6779.

(4) Contatori, C.; Domingues, N. I.; Barreto, R. L.; de Lima, N. B.; Vatavuk, J.; Borges, A. A. C.; Almeida, G. F. C.; Couto, A. A. Effect of Mg and Cu on microstructure, hardness and wear on functionally graded Al-19Si alloy prepared by centrifugal casting. *J. Mater. Res. Technol.* **2020**, *9*, 15862−15873.

(5) Zhang, Z. H.; Sridhar, S.; Wei, G. Y.; Yu, Y. D.; Zhang, Z. Q.; Jiang, L.; Yang, Y. M.; Shahzad, M. W.; Chen, X.; Ben, B. X. A highly controlled fabrication of porous anodic aluminium oxide surface with versatile features by spatial thermo-anodization. *Surf. Coat. Technol.* **2021**, *408*, No. 126809.

(6) do Nascimento, J. P. L.; Ferreira, M. O. A.; Gelamo, R. V.; Scarminio, J.; Steffen, T. T.; da Silva, B. P.; Aoki, I. V.; dos Santos, A. G.; de Castro, V. V.; Malfatti, C. D.; Moreto, J. A. Enhancing the corrosion protection of Ti-6Al-4V alloy through reactive sputtering niobium oxide thin films. *Surf. Coat. Technol.* **2021**, *428*, No. 127854.

(7) Moreto, J. A.; Gelamo, R. V.; da Silva, M. V.; Steffen, T. T.; de Oliveira, C. J. F.; Buranello, P. A. A.; Pinto, M. R. New Insights of Nb$_2$O$_5$-Based coatings on the 316L SS surfaces: Enhanced biological responses. *J. Mater. Sci.: Mater. Med.* **2021**, *32*, No. 25.

(8) Bino, M. C. A.; Eurídice, W. A.; Gelamo, R. V.; Leite, N. B.; da Silva, M. V.; de Siervo, A.; Pinto, M. R.; Buranello, P. A. A.; Moreto, J. A. Structural and morphological characterization of Ti$_6$Al$_4$V alloy surface functionalization based on Nb$_2$O$_5$ thin film for biomedical applications. *Appl. Surf. Sci.* **2021**, *557*, No. 149739.

(9) Atrens, A.; Shi, Z. M.; Mehreen, S. U.; Johnston, S.; Song, G. L.; Chen, X. H.; Pan, F. S. Review of Mg alloy corrosion rates. *J. Magnesium Alloys* **2020**, *8*, 989−998.

(10) Wen, Y. Q.; Ma, M. M.; Baboukani, A. R.; Yang, J.; Macdonald, D. D.; Shang, W.; Wang, C. L. Microporous micro-arc oxidation/bis-[3-Triethoxysilylpropyl] tetrasulfide/graphene composite film with improved corrosion protection properties on aluminum alloy. *J. Alloys Compd.* **2021**, *871*, No. 159526.

(11) Moreto, J. A.; dos Santos, M. S.; Ferreira, M. O. A.; Carvalho, G. S.; Gelamo, R. V.; Aoki, I. V.; Taryba, M.; Bose Filho, W. W.; Fernandes, J. C. S. Corrosion and corrosion-fatigue synergism on the base metal and nugget zone of the 2524-T3 Al alloy joined by FSW process. *Corros. Sci.* **2021**, *182*, No. 109253.

(12) Freitas, L. R.; Gelamo, R. V.; Marino, C. E. B.; Nascimento, J. P. L.; Figueiredo, J. M. A.; Fernandes, J. C. S.; Moreto, J. A. Corrosion behaviour of reactive sputtering deposition niobium oxide based coating on the 2198-T851 aluminium alloy. *Surf. Coat. Technol.* **2022**, *434*, No. 128197.

(13) Ferreira, M. O. A.; Gelamo, R. V.; Marino, C. E. B.; da Silva, B. P.; Aoki, I. V.; da Luz, M. S.; Alexopoulos, N. D.; Leite, N. B.; Moreto, J. A. Effect of niobium oxide thin film on the long-term immersion corrosion of the 2198-T851 aluminium alloy. *Materialia* **2022**, *22*, No. 101407.

(14) Moreto, J. A.; Gelamo, R. V.; Nascimento, J. P. L.; Taryba, M.; Fernandes, J. C. S. Improving the corrosion protection of 2524-T3-Al alloy through reactive sputtering Nb_2O_5 coatings. *Appl. Surf. Sci.* **2021**, *556*, No. 149750.

(15) Li, X. J.; Yin, S. H.; Luo, H. Fabrication of robust superhydrophobic $Ni-SiO_2$ composite coatings on aluminum alloy surfaces. *Vacuum* **2020**, *181*, No. 109674.

(16) Liu, J. G.; Fang, X. T.; Zhu, C. Y.; Xing, X.; Cui, G.; Li, Z. L. Fabrication of superhydrophobic coatings for corrosion protection by electrodeposition: A comprehensive review. *Colloids Surf., A* **2020**, *607*, No. 125498.

(17) Ding, S.; Xiang, T.; Li, C.; Zheng, S.; Wang, J.; Zhang, M.; Dong, C.; Chan, W. Fabrication of self-cleaning super-hydrophobic nickel/graphene hybrid film with improved corrosion resistance on mild steel. *Mater. Des.* **2017**, *117*, 280−288.

(18) Yuan, G.; Liu, Y.; Ngo, C. V.; Guo, C. L. Rapid fabrication of anti-corrosion and self-healing superhydrophobic aluminum surfaces through environmentally friendly femtosecond laser processing. *Opt. Express* **2020**, *28*, 35636−35650.

(19) Shi, T.; Li, X. W.; Zhang, C. W.; Wang, H. X.; He, Z. Y.; Zhou, X. G.; Yang, D. N.; Zhang, B. B.; Yang, K. One-step preparation of the superhydrophobic Al alloy surface with enhanced corrosion and wear resistance. *Mater. Corros.* **2021**, *72*, 904−911.

(20) Lian, Z. X.; Xu, J. K.; Yu, P.; Yu, Z. J.; Wang, Z. B.; Yu, H. D. Oil-Repellent and corrosion resistance properties of superhydrophobic and superoleophobic aluminum alloy surfaces based on nanosecond laser-textured treatment. *Met. Mater. Int.* **2020**, *26*, 1603−1610.

(21) Nhung Nguyen, T. P.; Brunet, P.; Coffinier, Y.; Boukherroub, R. Quantitative testing of robustness on super-omniphobic surfaces by drop impact. *Langmuir* **2010**, *26*, 18369−18373.

(22) Wong, T. S.; Kang, S. H.; Tang, S. K. Y.; Smythe, E. J.; Hatton, B. D.; Grinthal, A.; Aizenberg, J. Bioinspired self-repairing slippery surfaces with pressure-stable omniphobicity. *Nature* **2011**, *477*, 443−447.

(23) Gulfam, R.; Zhang, P. Power generation and longevity improvement of renewable energy systems via slippery surfaces-a review. *Renew. Energy* **2019**, *143*, 922−938.

(24) Wu, D. Q.; Ma, L. W.; Zhang, F.; Qian, H. C.; Minhas, B.; Yang, Y. M.; Han, X.; Zhang, D. W. Durable deicing lubricant-infused surface with photothermally switchable hydrophobic/slippery property. *Mater. Des.* **2019**, *185*, No. 108236.

(25) Wang, Z. H.; Scheres, L.; Xia, H. S.; Zuilhof, H. Developments and challenges in self-healing antifouling materials. *Adv. Funct. Mater.* **2020**, *30*, No. 1908098.

(26) Lian, Z. X.; Xu, J. K.; Wang, Z. B.; Yu, H. D. Biomimetic superlyophobic metallic surfaces: Focusing on their fabrication and applications. *J. Bionic Eng.* **2020**, *17*, 1−33.

(27) Inoue, T.; Koyama, A.; Kowalski, D.; Zhu, C. Y.; Aoki, Y.; Habazaki, H. Fluorine-free slippery liquid-infused porous surfaces prepared using hierarchically porous aluminum. *Phys. Status Solidi* **2020**, *217*, No. 1900836.

(28) Ouyang, Y. B.; Zhao, J.; Qiu, R.; Hu, S. G.; Niu, H. L.; Zhang, Y.; Chen, M. Nanowall enclosed architecture infused by lubricant: A bio-inspired strategy for inhibiting bio-adhesion and bio-corrosion on stainless steel. *Surf. Coat. Technol.* **2020**, *381*, No. 125143.

(29) Sun, H. Y.; Lei, F.; Li, T.; Han, H.; Li, B.; Li, D. D.; Sun, D. Z. Facile fabrication of novel multifunctional lubricant-infused surfaces

with exceptional tribological and anticorrosive properties. *ACS Appl. Mater. Interfaces* **2021**, *13*, 6678−6687.

(30) Song, T. T.; Liu, Q. L.; Zhang, M. L.; Chen, R. R.; Takahashi, K.; Jing, X. Y.; Liu, L. H.; Wang, J. Multiple sheet-layered super slippery surfaces based on anodic aluminium oxide and its anticorrosion property. *RSC Adv.* **2015**, *5*, 70080−70085.

(31) Tuo, Y. J.; Zhang, H. F.; Chen, W. P.; Liu, X. W. Corrosion protection application of slippery liquid-infused porous surface based on aluminum foil. *Appl. Surf. Sci.* **2017**, *423*, 365−374.

(32) Luo, H.; Yin, S. H.; Huang, S.; Chen, F. J.; Tang, Q. C.; Li, X. J. Fabrication of slippery Zn surface with improved water-impellent, condensation and anti-icing properties. *Appl. Surf. Sci.* **2019**, *470*, 1139−1147.

(33) Sun, J.; Wang, C.; Song, J. L.; Huang, L.; Sun, Y. K.; Liu, Z. A.; Zhao, C. L.; Li, Y. X. Multi-functional application of oil-infused slippery Al surface: From anti-icing to corrosion resistance. *J. Mater. Sci.* **2018**, *53*, 16099−16109.

(34) Ouyang, Y. B.; Zhao, J.; Qiu, R.; Hu, S. G.; Chen, M.; Wang, P. Liquid-infused superhydrophobic dendritic silver matrix: A bio-inspired strategy to prohibit biofouling on titanium. *Surf. Coat. Technol.* **2019**, *367*, 148−155.

(35) Qiu, Z. H.; Qiu, R.; Xiao, Y. M.; Zheng, J. Y.; Lin, C. G. Slippery liquid-infused porous surface fabricated on CuZn: A barrier to abiotic seawater corrosion and microbiologically induced corrosion. *Appl. Surf. Sci.* **2018**, *457*, 468−476.

(36) Nguyen, T. B.; Park, S.; Jung, Y.; Lim, H. Effects of hydrophobicity and lubricant characteristics on anti-icing performance of slippery lubricant-infused porous surfaces. *J. Ind. Eng. Chem.* **2019**, *69*, 99−105.

(37) Xiang, T. F.; Zheng, S. L.; Zhang, M.; Sadig, H. R.; Li, C. Bio-inspired slippery zinc phosphate coating for sustainable corrosion protection. *ACS Sustainable Chem. Eng.* **2018**, *6*, 10960−10968.

(38) Geraldi, N. R.; Guan, J. H.; Dodd, L. E.; Maiello, P.; Xu, B. B.; Wood, D.; Newton, M. I.; Wells, G. G.; McHale, G. Double-sided slippery liquid-infused porous materials using conformable mesh. *Sci. Rep.* **2019**, *9*, No. 13280.

(39) Zhang, M. L.; Chen, R. R.; Liu, Q.; Liu, J. Y.; Yu, J.; Song, D. L.; Liu, P. L.; Gao, L. T.; Wang, J. Long-term stability of a liquid-infused coating with anti-corrosion and anti-icing potentials on al alloy. *ChemElectroChem* **2019**, *6*, 3911−3919.

(40) Zhang, M. L.; Liu, Q.; Chen, R. R.; Chen, H. L.; Song, D. L.; Liu, J. Y.; Zhang, H. S.; Li, R. M.; Wang, Y. L.; Wang, J. Lubricant-infused coating by double-layer ZnO on aluminium and its anti-corrosion performance. *J. Alloys Compd.* **2018**, *764*, 730−737.

(41) Vorobyev, A. Y.; Guo, C. L. Direct femtosecond laser surface nano/microstructuring and its applications. *Laser Photonics Rev.* **2013**, *7*, 385−407.

(42) Ta, V. D.; Dunn, A.; Wasley, T. J.; Li, J.; Kay, R. W.; Stringer, J.; Smith, P. J.; Esenturk, E.; Connaughton, C.; Shephard, J. D. Laser textured superhydrophobic surfaces and their applications for homogeneous spot deposition. *Appl. Surf. Sci.* **2016**, *365*, 153−159.

(43) Long, J. Y.; Zhong, M. L.; Zhang, H. J.; Fan, P. X. Superhydrophilicity to superhydrophobicity transition of picosecond laser microstructured aluminum in ambient air. *J. Colloid Interface Sci.* **2015**, *441*, 1−9.

(44) Fang, Y.; Yong, J. L.; Cheng, Y.; Yang, Q.; Hou, X.; Chen, F. Liquid-infused slippery stainless steel surface prepared by alcohol-assisted femtosecond laser ablation. *Adv. Mater. Interfaces* **2021**, *8*, No. 2001334.

(45) Song, J. L.; Pan, W. H.; Wang, K.; Chen, F. Z.; Sun, Y. W. Fabrication of micro-reentrant structures by liquid/gas interface shape-regulated electrochemical deposition. *Int. J. Mach. Tools Manuf.* **2020**, *159*, No. 103637.

(46) Lu, Y.; Guan, Y. C.; Li, Y.; Yang, L. J.; Wang, M. L.; Wang, Y. Nanosecond laser fabrication of superhydrophobic surface on 316L stainless steel and corrosion protection application. *Colloids Surf., A* **2020**, *604*, No. 125259.

(47) Wang, G.; Shen, Y.; Tao, J.; Luo, X.; Zhang, L.; Xia, Y. Fabrication of a superhydrophobic surface with a hierarchical

nanoflake-micropit structure and its anti-icing properties. *RSC Adv.* **2017**, *7*, 9981−9988.

(48) Liu, R.; Chi, Z. D.; Cao, L.; Weng, Z. K.; Wang, L.; Li, L.; Saeed, S.; Lian, Z. X.; Wang, Z. B. Fabrication of biomimetic superhydrophobic and anti-icing Ti6Al4V Alloy surfaces by direct laser interference lithography and hydrothermal treatment. *Appl. Surf. Sci.* **2020**, *534*, No. 147576.

(49) Wenzel, R. N. Surface roughness and contact angle. *J. Phys. Chem. A* **1949**, *53*, 1466−1467.

(50) Lou, R.; Li, G. Y.; Wang, X.; Zhang, W. F.; Wang, Y. S.; Zhang, G. D.; Wang, J.; Cheng, G. H. Antireflective and superhydrophilic structure on graphite written by femtosecond laser. *Micromachines* **2021**, *12*, 236.

(51) Nishino, T.; Meguro, M.; Nakamae, K.; Matsushita, M.; Ueda, Y. The lowest surface free energy based on -CF3 alignment. *Langmuir* **1999**, *15*, 4321−4323.

(52) Samanta, A.; Huang, W.; Chaudhry, H.; Wang, Q.; Shaw, S. K.; Ding, H. Design of chemical surface treatment for laser textured metal alloy to achieve extreme wetting behavior. *ACS Appl. Mater. Interfaces* **2020**, *12*, 18032−18045.

(53) Ensikat, H. J.; Ditsche-Kuru, P.; Neinhuis, C.; Barthlott, W. Superhydrophobicity in perfection: The outstanding properties of the lotus leaf. *Beilstein J. Nanotechnol.* **2011**, *2*, 152−161.

(54) Ferrari, M.; Benedetti, A. Superhydrophobic surfaces for applications in seawater. *Adv. Colloid Interface Sci.* **2015**, *222*, 291−304.

(55) Yao, W. H.; Wu, L.; Sun, L. D.; Jiang, B.; Pan, F. S. Recent developments in slippery liquid-infused porous surface. *Prog. Org. Coat.* **2022**, *166*, No. 106806.

(56) Heydarian, S.; Jafari, R.; Momen, G. Recent Progress in the anti-icing performance of slippery liquid-infused surfaces. *Prog. Org. Coat.* **2021**, *151*, No. 106096.

(57) Stern, M.; Geaby, A. L. Electrochemical polarization. *J. Electrochem. Soc.* **1957**, *104*, No. 56.

(58) Trdan, U.; Sano, T. K.; Klobcar, D. J.; Sano, Y. J.; Grum, J.; Sturm, R. Improvement of corrosion resistance of AA2024-T3 using femtosecond laser peening without protective and confining medium. *Corros. Sci.* **2018**, *143*, 46−55.

(59) Jayaraj, J.; Raj, S. A.; Srinivasan, A.; Ananthakumar, S.; Pillai, U. T. S.; Dhaipule, N. G. K.; Mudali, U. K. Composite magnesium phosphate coatings for improved corrosion resistance of magnesium AZ31 alloy. *Corros. Sci.* **2016**, *113*, 104−115.

(60) Moreto, J. A.; Marino, C. E. B.; Bose Filho, W. W.; Rocha, L. A.; Fernandes, J. C. S. SVET, SKP and EIS study of the corrosion behaviour of high strength Al and Al-Li alloys used in aircraft fabrication. *Corros. Sci.* **2014**, *84*, 30−41.

(61) Baux, J.; Causse, N.; Esvan, J.; Delaunay, S.; Tireau, J.; Roy, M.; You, D.; Pebere, N. Impedance analysis of film-forming amines for the corrosion protection of a carbon steel. *Electrochim. Acta* **2018**, *283*, 699−707.

(62) Faure, M.; Billon, F.; Haghiri-Gosnet, A. M.; Tribollet, B.; Deslouis, C.; Pailleret, A.; Gamby, J. Influence of the atomic nitrogen content in amorphous carbon nitride thin films on the modulation of their polarizable interfaces properties. *Electrochim. Acta* **2018**, *280*, 238−247.

(63) Li, D. W.; Wang, H. Y.; Liu, Y.; Wei, D. S.; Zhao, Z. X. Large-scale fabrication of durable and robust super-hydrophobic spray coatings with excellent repairable and anti-corrosion performance. *Chem. Eng. J.* **2019**, *367*, 169−179.

(64) Xhanari, K.; Finsgar, M. Organic corrosion inhibitors for aluminum and its alloys in chloride and alkaline solutions: A review. *Arabian J. Chem.* **2019**, *12*, 4646−4663.

(65) Li, X.; Jiang, Y.; Jiang, Z.; Li, Y.; Wen, C.; Zhang, D.; Lian, J.; Zhang, Z. Improvement of corrosion resistance of H59 brass through fabricating superhydrophobic surface using laser ablation and heating treatment. *Corros. Sci.* **2020**, *180*, No. 109186.

(66) Yu, P.; Lian, Z. X.; Xu, J. K.; Yu, H. D. Slippery liquid infused porous surfaces with corrosion resistance potential on aluminum alloy. *RSC Adv.* **2021**, *11*, 847−855.

(67) Wu, D.; Zhang, D.; Ye, Y.; Ma, L.; Minhas, B.; Liu, B.; Terryn, H. A.; Mol, J. M. C.; Li, X. Durable lubricant-infused anodic aluminum oxide surfaces with high-aspect-ratio nanochannels. *Chem. Eng. J.* **2019**, *368*, 138.

(68) Hasan, M. S.; Nosonovsky, M. Lotus Effect and Friction: Does Nonsticky Mean Slippery? *Biomimetics* **2020**, *5*, 28.

(69) Anandkumar, R.; Almeida, A.; Vilar, R. Wear behavior of Al-12Si/TiB2 coatings produced by laser cladding. *Surf. Coat. Technol.* **2011**, *205*, 3824−3832.

(70) Anandkumar, R.; Almeida, A.; Vilar, R. Microstructure and sliding wear resistance of an Al-12 Wt.% Si/TiC laser clad coating. *Wear* **2012**, *282−283*, 31−39.